Monthly Notices
of the
ROYAL ASTRONOMICAL SOCIETY

MNRAS **513,** 3387–3398 (2022)
Advance Access publication 2022 March 30

https://doi.org/10.1093/mnras/stac866

The scaling relation between galaxy luminosity and WHIM density from EAGLE simulations with application to SDSS data

Patrick Holt,[1]★ Toni Tuominen,[2] Jukka Nevalainen,[2] Massimiliano Bonamente,[1]★ Teet Kuutma,[2] Pekka Heinämäki[3] and E. Tempel[2]

[1]*Department of Physics, University of Alabama in Huntsville, Huntsville, AL 35899, USA*
[2]*Tartu Observatory, University of Tartu, Observatooriumi 1, Tõravere 61602, Estonia*
[3]*Tuorla Observatory, Department of Physics and Astronomy, University of Turku, Väisäläntie 5, 20014 Turku, Finland*

Accepted 2022 March 22. Received 2022 March 22; in original form 2021 October 7

ABSTRACT

This paper presents an updated scaling relation between the optical luminosity density (LD) of galaxies in the *r* band and the density of the warm–hot intergalactic medium (WHIM) in cosmic filaments, using the high-resolution EAGLE simulations. We find a strong degree of correlation between the WHIM density and the galaxy luminosity density, resulting in a scaling relation between the two quantities that permits us to predict the WHIM density of filaments with a scatter of less than $\frac{1}{2}$ dex in a broad range of smoothed filament luminosity densities. In order to estimate the performance of the simulation-based calibration of the LD–WHIM density relation, we applied it to a sample of low-redshift filaments detected with the *Bisous* method in the Legacy Survey SDSS DR12 data. In the volume covered by the SDSS data, our relation predicts a WHIM density amounting to $31 \pm 7 \pm 12$ per cent (statistical errors followed by systematic) of cosmic baryon density. This agrees, albeit within the large uncertainties, with the current estimates of the cosmological missing baryon fraction, implying that our LD–WHIM density relation may be a useful tool in the search for the missing baryons. This method of analysis provides a new promising avenue to study the physical properties of the missing baryons, using an observable that is available for large volumes of the sky, complementary and independent from WHIM searches with absorption-line systems in the FUV or X-rays.

Key words: intergalactic medium – large-scale structure of Universe – cosmology: observations.

1 INTRODUCTION: THE NEED TO USE GALAXY LUMINOSITY AS A TRACER OF WHIM BARYONS

The diffuse intergalactic medium contains the majority of the Universe's baryons at all redshifts (e.g. Shull, Smith & Danforth 2012). At high redshift, most of the baryons are in a photoionized phase that is primarily detected via the Lyman α forest (e.g. Penton, Shull & Stocke 2000). At low redshift, a large fraction of the baryons are expected to be in a warm–hot intergalactic medium (WHIM) phase at temperatures $\log T(K) = 5$–7 (Cen & Ostriker 1999; Davé et al. 2001; Bertone, Schaye & Dolag 2008; Martizzi et al. 2019). The low–temperature range of WHIM temperatures is effectively probed by the available FUV data, primarily *HST* and *FUSE*, revealing that FUV absorption lines (primarily O VI and the H I Lyman series) only trace a portion of the low-redshift baryons (Ostriker 1999; Davé et al. 2001; Bertone et al. 2008; Cen & Martizzi et al. 2019).

Shull et al. (2012) provided a popular census of the observational status of the cosmic baryon budget at low redshift, estimating that $\approx 30 \pm 10$ per cent of the baryons predicted by the concordance cosmology have not been detected. These results are later refined by Danforth et al. (2016), who estimated that the cosmic baryon density traced by O VI and H I with *HST*/COS, the most important elements detected in the FUV, is substantially lower than assumed in Shull et al. (2012). Consequently, the missing baryon density may amount to ∼50 per cent of the cosmic baryon density.

There are several serious uncertainties with the estimate of the total baryons traced by the FUV (see discussion in Tuominen et al. 2021). One key source of uncertainty is that the temperature and metal abundance of the gas are not known from observations. The conversion into the the associated hydrogen mass is done based on simulations and it can be uncertain by a factor of several. Another problem is that O VI can be detected in the same range of temperatures where H I broad Lyman α (BLA) lines occur, which is in the low end of the WHIM temperature range. One must therefore consider the possibility that a fraction of the baryons traced by O VI are the same baryons that were detected by BLA measurements. Finally, it is also possible that, due to the sensitivity limits of the COS surveys, the FUV has only probed the most dense circumgalactic medium (CGM) close to the galaxies. FUV studies do provide evidence that at least a portion of these O VI absorption lines are associated with the galaxies themselves (e.g. Stocke et al. 2006; Tchernyshyov et al. 2022). It is therefore possible that the warm WHIM (i.e. in the $\sim\log T(K) = 5$–6 range) in the cosmic filaments has not been detected yet, and thus it constitutes an additional missing baryon component. These considerations render the missing baryon fraction very uncertain. In this paper, we adopt the commonly accepted scenario that half of the cosmic baryon budget may be missing.

★ E-mail: bonamem@uah.edu (MB); psh0008@uah.edu (PH)

Simulations (e.g. EAGLE, Schaye et al. 2015; Tuominen et al. 2021, IllustrisTNG, Pillepich et al. 2018; Galárraga-Espinosa et al. 2021) indicate that a combination of hot WHIM (i.e, $\sim\log T(K) = 6$–7) and the FUV-detectable warm WHIM may be the missing WHIM. The high-temperature WHIM can be probed with X-ray lines such as those from O VII or O VIII, but the resolution of available X-ray instrumentation can only provide tentative detections of some of the more massive WHIM systems (e.g. Fang et al. 2010; Bonamente et al. 2016; Nicastro et al. 2018; Ahoranta et al. 2020). It is therefore necessary to provide alternative ways to investigate the location and cosmological density of WHIM baryons in the local universe.

A complementary way to investigate the missing baryons problem is by using the relatively easily obtainable optical luminosity density of galaxies in cosmic filaments as a tracer of the WHIM phase. The underlying physical argument responsible for the correlation between the galaxy light and WHIM density distribution is the dominating role of the gravitational potential of the dark matter concentrations at the filament spines. An important heating mechanism of the intergalactic baryons in the large-scale structure is the adiabatic compressional heating of the matter accreted towards the filaments. The baryons falling towards the filaments also experience shock-heating which is stronger closer to the maxima of the gravitational potential, i.e. the filament spines. Thus, the intergalactic medium is expected to be the hottest ($\log T(K) = 6$–7) within $\sim$1 Mpc of the filament spines, as demonstrated by Tuominen et al. (2021) with the EAGLE data.

The interaction of galaxies with the large-scale structure is very different. Yet, the galaxy density is highest at the filament spines (e.g. Galárraga-Espinosa et al. 2020), and galaxies are born at the maxima of the dark matter fluctuations. This is most likely to happen close to the filament spines, where the dark matter density is the highest. An initial investigation by Nevalainen et al. (2015) revealed a correlation between the luminosity density of galaxies and the WHIM density in the cosmological simulations of Cui et al. (2012). The resulting scaling relation between galaxy luminosity density (hereafter LD) and the WHIM density was successfully applied to filamentary structures in the Sculptor Wall supercluster, showing that the scaling relation is consistent with the available constraints from X-ray observations of the WHIM (Nevalainen et al. 2015). This preliminary study therefore provided confidence that the optical luminosity of galaxies can be used as a proxy for WHIM density.

In this paper we update the LD-WHIM scaling relation with state-of-the-art EAGLE simulations. Our goal is to apply it to such a large observational filament sample (from SDSS) so that an evaluation of the WHIM contribution to the cosmic baryon budget is feasible. This evaluation is necessary in order to test how well our relation performs in recovering the missing baryons in filaments. Our definition of the WHIM is gas outside r_{200} of haloes, and in the temperature range of $\log T(K) = 5$–7. The paper is structured as follows. Section 2 describes the EAGLE simulations used for the new evaluation of the LD-WHIM scaling relation. Section 3 describes the method of analysis of the WHIM simulations to obtain the new scaling relation. Section 4 presents our analysis of the cosmic baryon inventory by applying the LD–WHIM density relation to the SDSS filaments and Section 5 provides our conclusions.

2 EAGLE SIMULATIONS

The EAGLE project (Evolution and Assembly of GaLaxies and their Environments) is a suite of hydrodynamical simulations of the evolution of the universe (Schaye et al. 2015). EAGLE features the standard ΛCDM cold dark matter and dark energy cosmology, with the simulations run in volumes of 25 to 100 comoving Mpc (cMpc) sided cubes. The EAGLE simulations use state-of-the-art numerical techniques and subgrid models for radiative cooling, star formation, stellar mass-loss and metal enrichment, energy feedback from star formation, gas accretion on to, and mergers of, supermassive black holes and AGN feedback, including the calibration of subgrid feedback to observables (Crain et al. 2015). The galaxy data and snapshots of the EAGLE simulations are available to the public (McAlpine et al. 2016; The EAGLE team 2017).

EAGLE was run using a modified version of the *N*-body Tree-PM smoothed particle hydrodynamics (SPH) code Gadget 3 (Springel 2005), with the main modifications being the formulation of SPH, the time-steps, and the subgrid physics. Of the available EAGLE simulations, we use the largest simulation (Ref-L0100N1504) at a redshift of $z = 0$. The simulation has a comoving box size of 100 cMpc, a total of 2×1504^3 particles, an initial baryonic particle mass of $1.81 \times 10^6 M_\odot$, a dark matter particle mass of $9.7 \times 10^6 M_\odot$, comoving Plummer-equivalent gravitational softening length of 2.66 ckpc, and the maximum physical softening length value of 0.70 kpc. This is the same EAGLE simulation used by Tuominen et al. (2021) for the investigation of the missing baryons in the local Universe.

2.1 Constructing the WHIM density and temperature grid

The baryon particles in the simulation, along with the associated mass, temperature, and density for each particle, were used to create a 500^3 uniform grid that forms the basic data set we use for this study. Since our interest is in the diffuse warm–hot intergalactic medium, we excluded particles in bound structures, namely those within R_{200} of a virialized structure as identified by a friends–of–friends halo given in the EAGLE data base (McAlpine et al. 2016). Each grid point is therefore representative of a cubic cell of volume $V = 0.2^3$ Mpc^3 with a mass equal to the sum of the masses of all particles outside r_{200} within the j–th cell,

$$M_j = \sum_i m_i (r > r_{200}). \tag{1}$$

Using the temperature of each particle not within a bound structure, we calculated the mean mass–weighted weighted temperature for each cell j,

$$T_j = \frac{1}{M_j} \sum_i m_i (r > r_{200}) \cdot T_i (r > r_{200}). \tag{2}$$

To evaluate the density of the intergalactic WHIM, we need to estimate the portion of the volume of the cell occupied by virialized structures. For this purpose, we take the mass $m_{b,\,i} = m_i (r \leq r_{200})$ of each bound particle and divided it by the particle density $\rho_{b,\,i}$, so that the volume occupied by bound structures in each cell is

$$V_{b,j} = \sum_i \frac{m_{b,i}}{\rho_{b,i}}. \tag{3}$$

Next, we calculate the WHIM density for each grid point using all particles, and selecting cells with an average temperatures within the WHIM range, $\log T(K) = 5$–7, resulting in

$$\rho_{j,\mathrm{WHIM}} = \frac{M_j}{V - V_{b,j}}. \tag{4}$$

To complete the construction of the WHIM density cube, we have to exclude temperatures outside the WHIM temperature range, which we chose as $\log T(K) = 5$–7. For grid points with T_j values outside the WHIM temperature range, we set the mass density equal to zero. Figs 6 and 5 in Tuominen et al. (2021) show examples of

Table 1. Main statistics of filaments, WHIM, and LD properties in the EAGLE simulations at $z = 0$, and associated cosmological quantities. Throughout this paper we use the *Planck* cosmological parameters that are presented in Planck Collaboration XVI (2014).

Number of cells	125 000 000
Total volume	100^3 Mpc^3
Individual cell volume	0.2^3 Mpc^3
Number and fraction of cells in *Bisous* filaments	6 267 543 (5.0 per cent)
Number and fraction of cells in WHIM ($5 \leq \log T(K) \leq 7$)	4 263 052 (3.3 per cent)
Average LD in EAGLE	$7.1 \times 10^7 L_\odot$ Mpc^{-3}
WHIM mass in filaments	$2.15 \times 10^{15} M_\odot$
Baryon fraction of WHIM in *Bisous* filaments	$\Omega_{\rm WHIM,\,fil} = 0.35$
Hot WHIM ($6 \leq \log T(K) \leq 7$) mass in *Bisous* filaments	$0.86 \times 10^{15} M_\odot$
Adopted baryon density	$\Omega_b = 0.05$
Adopted Hubble constant (from *Planck*)	$H_0 = 67.8$ km s^{-1} Mpc^{-1}
Mean baryon density (from *Planck*)	$\overline{\rho_b} = \frac{3H_0^2}{8\pi G}\Omega_b = 0.618 \times 10^{10}M_\odot$Mpc^{-3}

the WHIM density and temperature map in the EAGLE simulations obtained following this method. One of the advantages of mapping the EAGLE simulations into a regular grid is the ease of comparison with observational data, as shown in Section 4.

2.2 Galaxy filaments

We adopted the EAGLE filaments of galaxies identified in Tuominen et al. (2021) and Kuutma et al. (2020) using the *Bisous* method devised by Stoica, Martínez & Saar (2007) and successfully applied to various numerical simulations (Tempel et al. 2014a; Nevalainen et al. 2015; Muru & Tempel 2021). The Bisous method uses connected cylindrical volumes to identify coherent galaxy structures that can be identified as filament network. The current implementation of the Bisous method models the galaxy distributions with connected cylinders of a relatively narrow range of radii (0.5–1.0 Mpc), the EAGLE sample average being at ∼0.75 Mpc. The process was repeated 1000 times to account for the stochastic nature of the Bisous formalism. The locations that are more often covered by the cylinders in the individual runs are more likely to belong to a filament. At the locations of the filament spines, the rate of coverage by the cylinder reaches the local maxima. The boundaries of a given filament, which we need in order to capture the diffuse LD and WHIM within filaments, are drawn at a location around the filament spine where the rate of the cylinder coverage decreases below an experimentally set limit, chosen in such a way that it yielded the statistical properties of the SDSS filaments (see Tempel et al. 2014b for additional details).

Tuominen et al. (2021) showed that these choices result in EAGLE filaments that have a typical radius on 1 Mpc. The main statistics of the filaments, LD, and WHIM for the entire EAGLE volume are provided in Table 1.

2.3 Constructing the luminosity density grid

The primary goal of this study is to use the galaxy luminosity as a proxy for the WHIM density field. For this purpose we follow closely the procedure described in Tuominen et al. (2021) to generate a smoothed luminosity density (LD) field with the positions and r-band luminosities of all EAGLE galaxies with $M_r \leq -18.4$. We adopted the galaxy sample and luminosities from Kuutma et al. (2020), i.e. for each galaxy we used the magnitude with dust attenuation as described in Camps et al. (2018) if such value was available. Otherwise we used the dust-free magnitudes. This approach yielded an average r-band LD of $<\mathrm{LD}> = 7.1 \times 10^7$ L$_\odot$ Mpc^{-3} (Tuominen et al. 2021).

Such a choice of M_r in EAGLE mimics the number density of SDSS galaxies with a limiting magnitude of $M_r = -19$ at $z = 0.05$. In order to recreate a comparable filamentary network, it is essential to use galaxy samples with the same number density of galaxies. Using the same magnitude cut for EAGLE and SDSS would leave the former with a lower density of galaxies, changing the properties of the obtained filaments. Since $M_r = -19$ for SDSS galaxies effectively limits the distance up to where a complete filament network has been constructed for *Bisous* (Tempel et al. 2014b), we selected $M_r \leq -18.4$ for EAGLE to produce similar filaments.

A necessary step to compare the diffuse WHIM with the galaxy luminosity is to smooth the LD distribution on scales that are comparable to those of the WHIM. For this purpose, we continue to follow Tuominen et al. (2021) and smooth the galaxy luminosity with a B_3 spline kernel (Liivamägi, Tempel & Saar 2012). We then evaluate the continuous LD field in cells with a regular grid of size 0.2 Mpc on each side, same as for the WHIM density of Section 2.1. An example of an LD grid overlaid on the WHIM density fields is shown in Fig. 1, highlighting the spatial overlap between the smoothed LD and the WHIM density that it is intended to trace.

3 THE LD-WHIM SCALING RELATION

3.1 Defining the scaling relation

Following Nevalainen et al. (2015), we seek a relation between the LD and the WHIM density. We do this in terms of the luminosity overdensity, defined as

$$\delta_{\rm LD} = \frac{\rm LD}{\langle \rm LD \rangle},$$

where $\langle \mathrm{LD} \rangle$ is the mean luminosity density in the r-band of the full EAGLE simulation, and the WHIM overdensity,

$$\delta_\rho = \frac{\rho_{\rm WHIM}}{\overline{\rho_b}},$$

where $\overline{\rho_b}$ is the mean cosmic baryon density (see Table 1). In Nevalainen et al. (2015), the model chosen for the LD-WHIM relation was a power-law model

$$\delta_\rho = A\,\delta_{\rm LD}^B$$

featuring $A = 0.7 \pm 0.1$ and $B = 0.9 \pm 0.2$ as the best-fitting values and standard deviations of the two adjustable parameter.

In this paper, we choose to work with the logarithm of the LD and WHIM density data. On a logarithmic scale, the same power-law model becomes a linear model.

$$\log \delta_\rho = \log A + B\,\log \delta_{\rm LD}, \tag{5}$$

where the free parameter are now $\log A$ and B, the latter remaining the same between our analysis and that of Nevalainen et al. (2015). The use of the linear model (5) requires the transformation of the LD and the WHIM density to logarithmic scales before the fit, and therefore the exclusion of cells with zero values. As discussed below, the LD of interest is $\delta_{\rm LD} > 1$, and therefore only a negligible fraction of cells with $\delta_\rho = 0$ are excluded.

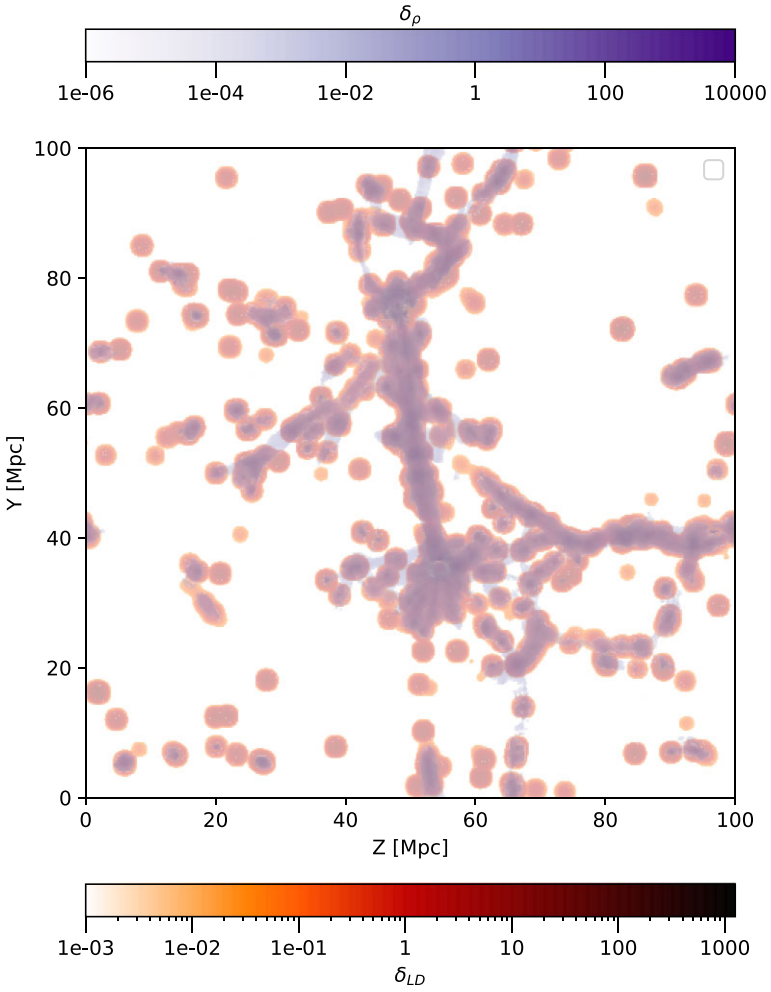

Figure 1. Image of 5 Mpc thick slice of the WHIM and LD within temperature range $T = \log 5$–7. The blue colours trace the WHIM, and red colours trace the smoothed luminosity density of galaxies.

3.2 Finding the optimal LD smoothing scale

Our Bisous method is tuned to detect the galaxy filament network at $\sim$ 1–2 Mpc width scales, since it is expected that this is the characteristic scale of the dominant galaxy filaments (see e.g. Tempel et al. 2014b,c,a, 2016.) However, the gas and galaxies are different physical entities and thus it is not obvious that the value of the optimal LD smoothing kernel radius equals the average Bisous cylinder radius of 0.75 Mpc. Thus, to optimize our methods, our task is to find what LD smoothing scale yields the best correlation between the smoothed LD and the WHIM distribution in the filaments detected with our current Bisous setting.

For this purpose we start by generating 50 smoothed LD fields using a range $a = 0.1$–5 Mpc of smoothing kernel radii, with a step size of 0.1 Mpc. We then computed the Pearson linear correlation coefficient between the LD grids and the WHIM density grid, as a function of a. Since our interest is in establishing a power-law relationship between LD and WHIM density, as defined in (5), the appropriate measure of the degree of correlation is the linear coefficient between the logarithm of the two quantities. In fact, the Pearson coefficient is equal to the product $r^2 = b \cdot b'$, where b and b' are the slopes of the linear regression of y on x, and of x on y, respectively (Bonamente 2017). It is therefore appropriate to evaluate the correlation coefficient for the logarithm of the quantities, since the scaling relation of interest is a linear function in the logarithms of the two quantities, see equation (5) above. The results of this analysis are shown in Fig. 2.

At the smallest values of the smoothing kernel radius, the light is scattered to very small distances from the galaxies. Since the diffuse WHIM fills the filaments well, most of the WHIM in filaments will not be traced with LD (i.e. many of the cells with large WHIM density have zero LD). This is reflected to a low correlation coefficient (see Fig. 2). The increasing smoothing scale increases the correlation coefficient, which peaks at $a \sim 1.2$ Mpc (see Fig. 2), i.e. at a somewhat higher scale than the average cylinder radius of 0.75 Mpc used for modelling the galaxy distribution when detecting the filaments with the Bisous method. The correlation is highly significant. At higher scales, an increasing fraction of the light is scattered towards WHIM-poor voids, leading to a lower correlation coefficient. We thus adopted $a = 1.2$ Mpc as the LD smoothing kernel radius. We will evaluate the resulting scatter of the traced WHIM in Section 3.3 obtained with this choice. Application of a different kernel radius would yield a lower correlation coefficient, i.e. lead to a larger scatter between the LD and WHIM. Our analysis therefore suggests the use of the $a = 1.2$ Mpc kernel, and that significantly different values of the kernel size will reduce the correlation between the WHIM density and the luminosity density.

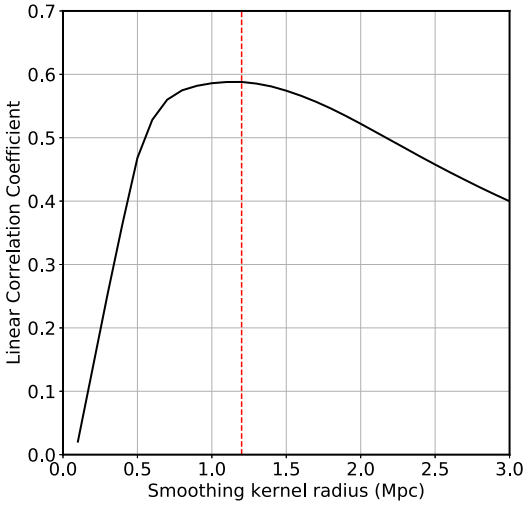

Figure 2. Linear correlation coefficient between the logarithms of the luminosity density and WHIM density, as a function of LD smoothing kernel radius a. The maximum is for $a = 1.2$ Mpc, marked by the dashed red line.

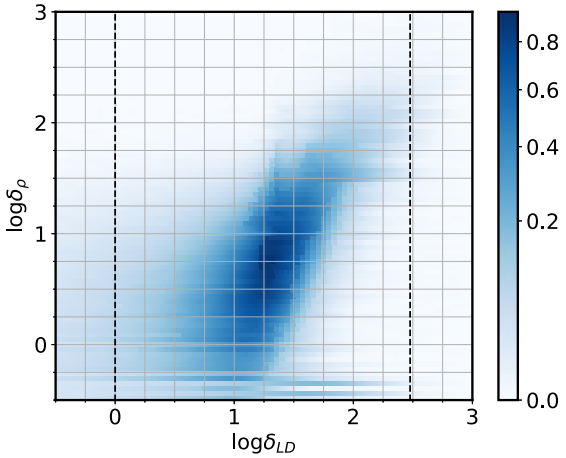

Figure 3. Distribution of LD overdensity and WHIM overdensity for $a = 1.2$ Mpc, illustrating the positive correlation between the two quantities. The darker colours indicate larger frequency of occurrence (numbers are frequency density). The vertical lines indicate the LD range we selected for the further analysis $\delta_{LD} = 1$–300.

The 2D distribution of the logarithms of the WHIM overdensity and luminosity overdensity are shown in Fig. 3, for the adopted smoothing parameter $a = 1.2$ Mpc. As expected, the higher LD corresponds to higher WHIM densities, and the strong degree of positive correlation between the two quantities is evident. The correlation is less evident at the lowest densities. Typically, cells with baryon densities that are just a few times the cosmic average are found close to the filament boundaries, approximately at a 1 Mpc distance from the filament spines (Tuominen et al. 2021, fig. 15). Beyond the filament boundary the baryon density drops to underdense levels, and at a distance of ∼4 Mpc the WHIM densities reach on average the voids which are underdense by a factor of ∼10. Since the filament boundaries do not have a fixed radius, smoothing with a fixed-radius kernel with $a = 1.2$ Mpc results in the possibility that a fraction of the luminosity density falls beyond the boundary of a thinner filament, thus leading to a larger scatter in the correlation between WHIM density and the smoothed galaxy luminosity density, and therefore

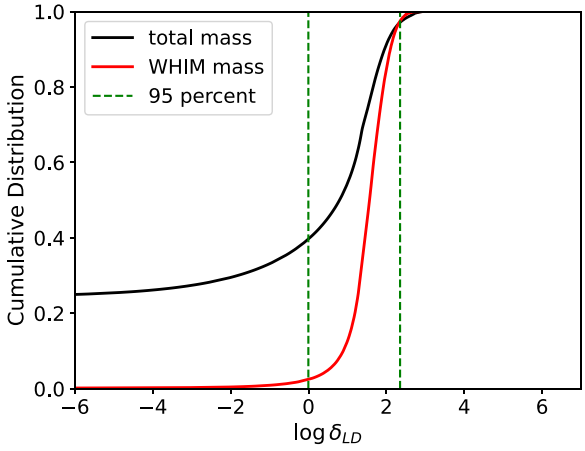

Figure 4. Cumulative distribution of WHIM mass as a function of the luminosity overdensity, for $a = 1.2$ Mpc, with the 95 per cent range indicated by green solid lines. For comparison, we also plot the distribution of mass of all the intergalactic medium, with ∼25 per cent of its mass in cells of $\delta_{LD} = 0$.

Table 2. Range of the logarithm of the luminosity overdensity δ_{LD} that include 95 per cent of the WHIM mass. For comparison, it is also reported the percent of mass included in the LD limits of Nevalainen et al. (2015).

a	95 percentiles (log δ_{LD})		No. zeros in LD		Per cent mass in LD = 0.01–2
			Filaments	Whole box	
1.0	−0.85	2.44	390361	99727119	0.93
1.2	−0.006	2.35	147129	88419657	0.96
1.5	0.4	2.24	25627	70396352	0.98
2.0	0.55	2.09	271	42720903	0.995

the lower correlation coefficient observed in Fig. 3 at the smallest values of the luminosity overdensity. On the other hand, cells with a density contrast $\delta_{LD} = 10$–100 are closer to the filament spines, and there the data do not suffer from the boundary effect; as a result, the correlation is stronger (see top right portion of the distribution in Fig. 3).

3.3 The LD-WHIM scaling relation from EAGLE

To determine the optimal LD interval range to be used in the scaling relation, we evaluated the cumulative distribution of the WHIM mass in filaments as a function of the luminosity overdensity δ_{LD}, shown in Fig. 4 for $a = 1.2$. For this value of the smoothing parameter, 95 per cent of the WHIM mass is included in cells with a luminosity overdensity of approximately $\delta_{LD} \simeq 1$–224. The luminosity overdensity range for other smoothing values are shown in Table 2. The range of luminosities chosen by Nevalainen et al. (2015) to encompass 95 per cent of the mass in their simulations, i.e. 0.01–2 $\times 10^{10}$ $L_\odot$ Mpc^{-3}, corresponds to a very similar range of luminosity overdensities, indicating a broad agreement with the earlier results. Since (i) we are not interested in underdense voids and (ii) Fig. 4 shows that there is very little WHIM at the highest densities (i.e. outside the virial regions of galaxies), we choose a luminosity overdensity range of $\delta_{LD} = 1$–300 for the evaluation of the scaling relation. The uncertainties associated with this choice are also evaluated in Section 3.4.

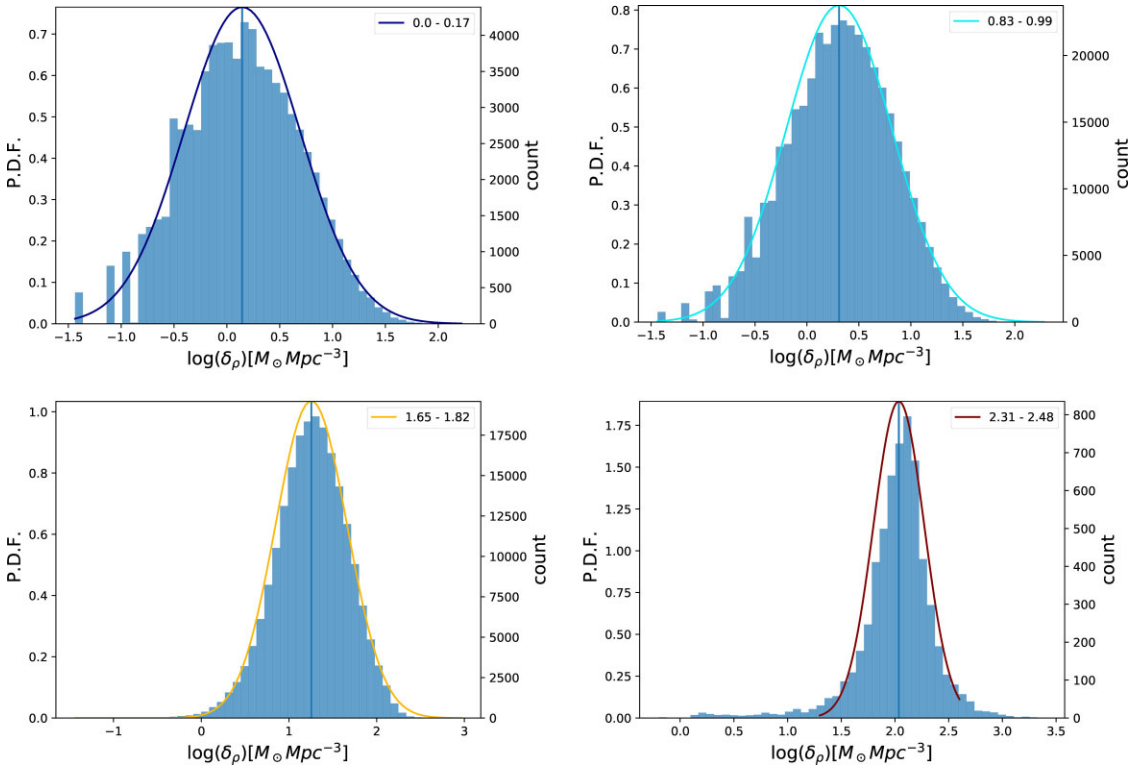

Figure 5. Sample distribution of WHIM overdensity accumulated within the $\log \delta_{\rm LD}$ range indicated in the top right-hand corner of the panel. For the two bins with the largest LD values, the distribution has tails that are not well described by the lognormal model, as shown in the bottom right-hand panel. For these two distributions we chose to exclude the extreme portions of the tails of the distributions in order to provide a reasonable approximation to the bulk of the WHIM density values with the lognormal model (the range that was excised was chosen ad–hoc, where the bins contained only few counts; the range in use corresponds to the support of the solid curve). For the lowest LD bins, the left wing of the distribution has sparse coverage, in correspondence to the horizontal stripes visible also in Fig. 3.

We then subdivide the LD range that $\delta_{\rm LD} = 1$–300 into 15 equally spaced logarithmic bins as in Nevalainen et al. (2015), and find the conditional probability distribution of the WHIM density in each of the 15 LD bins. The choice of binning according to LD values is suggested by the need to reduce the correlation among neighbouring ($\log \delta_{\rm LD}$, $\log \delta_\rho$) datapoints, while retaining a sufficiently large number of bins for the sake of an accurate determination of the two–parameter relation. In fact, both quantities are implicitly dependent on the underlying dark matter distribution, which drives the formation of both the WHIM filaments and the galaxies. To characterize the distribution of the WHIM density in each LD bin we fit the distribution of WHIM overdensities δ_ρ with a log-normal model, as in Nevalainen et al. (2015), which is a more satisfactory choice than a simple normal model, as illustrated in Fig. 5 for few representative LD bins. The result of all 15 LD bins are shown in Fig. 6 and Table 3.

We want to characterize the relationship between $\log \delta_{\rm LD}$ and $\log \delta_\rho$ with the simple linear model of equation (5). We also determine its uncertainty or confidence band, noting that such characterization of the best-fitting uncertainties will not be used for uncertainties in the derived quantities, such as the estimated WHIM mass, which will be done in Section 4. With the lognormal conditional probability distributions of $\log \delta_\rho$ for a fixed value of $\delta_{\rm LD}$, or $f(\log \delta_\rho / \delta_{{\rm LD},\,i})$, we are ready to obtain the best-fitting parameters for the scaling relation (5). Following Nevalainen et al. (2015), we perform a Monte Carlo sampling of the lognormal distribution of each LD bin to obtain a data set of 15 datapoints, and then for each sampled data set we perform a simple linear regression to the 15 data points and repeat this process 10 000 times. This Monte Carlo sampling of the conditional distributions provides the distributions of the two parameters of the linear model, and their covariance. The distribution of the best-fitting parameters $\log A$ and B are normal to a very good approximation, as shown in Fig. 7. We take the mean of each parameter's distribution as the best-fitting parameter value for our linear model, and the central 68 per cent confidence interval as the 1–σ uncertainty. Parameters of the scaling relation are reported in Table 4. This method of regression for the 15 LD bin data points is preferable to a standard regression of the weighted data points, since the conditional distributions functions are not independent measurements but correlated conditional distributions to which the standard method of linear regression is not directly applicable. The choice of 15 LD bins for use in the least-squares regression is the result of a heuristic choice that lets us model accurately the ($\delta_{\rm LD}$, δ_ρ) phase space with a simple two-parameter linear model that features an uncertainty (the green band in Fig. 8) that is well contained within the original scatter in the simulations (see the red dashed curves in Fig. 8, which correspond to the data of Table 3). The sampling from the 15 distributions also affords a simple method to provide an estimate for the uncertainties in derivative quantities, such as the predicted WHIM mass that is presented in Section 4.

The scaling relation is illustrated in Fig. 8, where the confidence band is obtained as the range that contains 68 per cent of the models from the 10 000 Monte Carlo samples used for the best fit. An equivalent confidence band can also be obtained from an error propagation of the $\log A$ and B parameters, at fixed values of the x–axis, which takes into account the covariance between the parameters (Bonamente 2017). In the range $\log \delta_{\rm LD} = 0$–2.5, corresponding

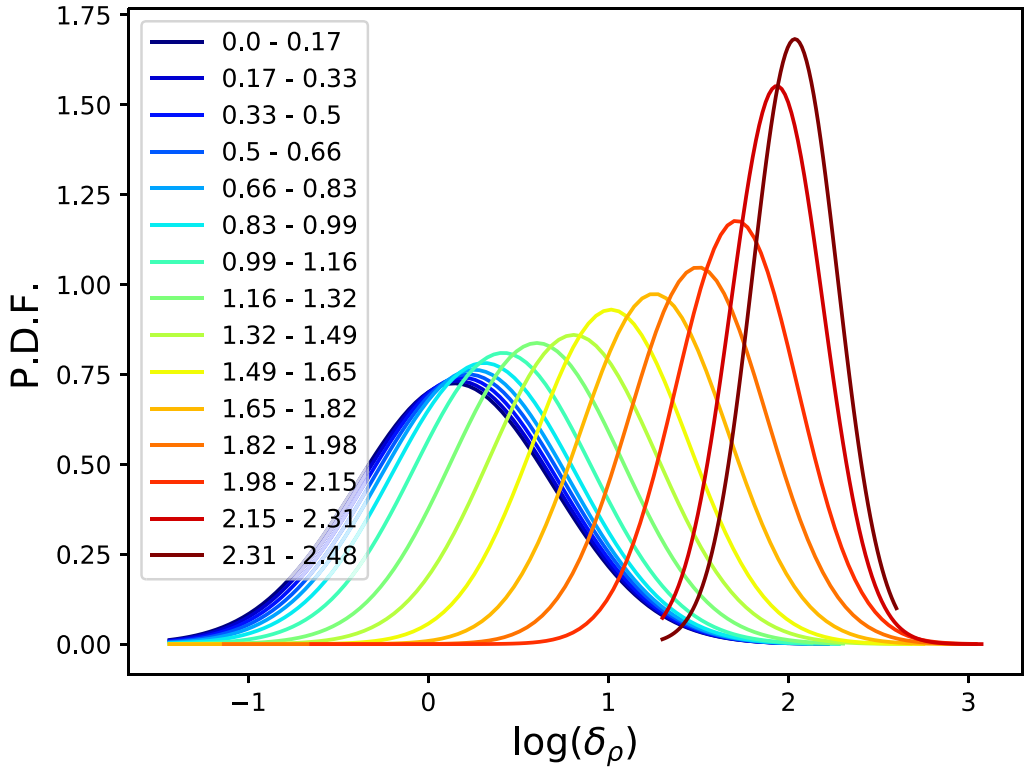

Figure 6. Probability distribution functions of the logarithm of the WHIM overdensity δ_ρ for each of the 15 bins, with smoothing $a = 1.2$ Mpc. In the plot legend, we indicated the range of bins 1–15 with their value of $\delta_{\rm LD}$. Notice how the distributions of the two highest LD bins have been truncated towards the tail, to prevent a small number of outlying datapoints to skew the lognormal fits.

Table 3. Log-normal values for each of the 15 distributions, using smoothing $a = 1.2$ Mpc.

Bin	Mean	Standard deviation	Number of cells
1	0.14	0.55	83820
2	0.16	0.54	109895
3	0.19	0.54	148395
4	0.22	0.53	205519
5	0.25	0.52	291723
6	0.31	0.51	412380
7	0.42	0.49	555065
8	0.60	0.48	662312
9	0.81	0.46	578294
10	1.01	0.43	404037
11	1.25	0.41	228770
12	1.50	0.38	112460
13	1.71	0.34	51394
14	1.94	0.26	21632
15	2.04	0.24	6899

approximately to overdensities LD = 1–300, the scaling relation predicts a WHIM density that varies by two orders of magnitude. The typical relative uncertainty in the prediction of the WHIM density at a fixed LD is given by the size of the green band, which is less than $\frac{1}{2}$ dex at all values of the luminosity density. This level of uncertainty will be reflected in the uncertainty in predicted WHIM masses when using the scaling relation. Notice how the best-fitting scaling relation for other values of the smoothing parameter in the range $a = 1$–2 Mpc fall comfortably within the 1–σ uncertainty of the $a = 1.2$ Mpc scaling relation.

3.4 Systematic biases and errors

The true WHIM filament mass in the entire EAGLE volume is 2.15×10^{15} M$_\odot$ (see Fig. 9), as obtained from a direct sum of all baryon particle masses in Bisous filaments and outside of r_{200}, and in the temperature range $\log T(K) = 5$–7, regardless of galaxy luminosity. To calibrate the LD-WHIM density scaling relation to reconstruct WHIM masses based on the galaxy LD, it is necessary to take into account the key choices made in the analysis and estimate biases and systematic errors associated with them. In the following, we investigate the effects of two key elements of the analysis, and how we correct for their biases and systematic errors.

3.4.1 Choice of smoothing kernel and LD range

The choice of a LD filter and the parameter a of the smoothing kernel are two key parameters used in the analysis. Table 5 shows the EAGLE WHIM masses using the LD range $\delta_{\rm LD} = 1$–300 (labelled 'LD mask'), which is a function of the smoothing parameter a, and the predicted WHIM mass using the same cells to which the scaling relation was applied ('Prediction from SR'). The uncertainty in the predicted masses from the scaling relation were obtained in the same manner as the green band from Fig. 8, i.e. by using 10 000 Monte Carlo 15-point samples. The results of the reconstruction of WHIM masses from the LD-WHIM scaling relations of Table 5 show that the nominal scaling relation for $a = 1.2$ does an excellent job at reconstructing the WHIM mass, with a small bias of ≤ -10 per cent (1.89×10^{15} M$_\odot$ versus 2.08×10^{15} M$_\odot$), when both the true WHIM mass and the one inferred by the scaling relations are limited to the LD range of $\delta_{\rm LD} = 1$–300 (see also Fig. 10). Although the agreement between the true EAGLE WHIM mass and that reconstructed from

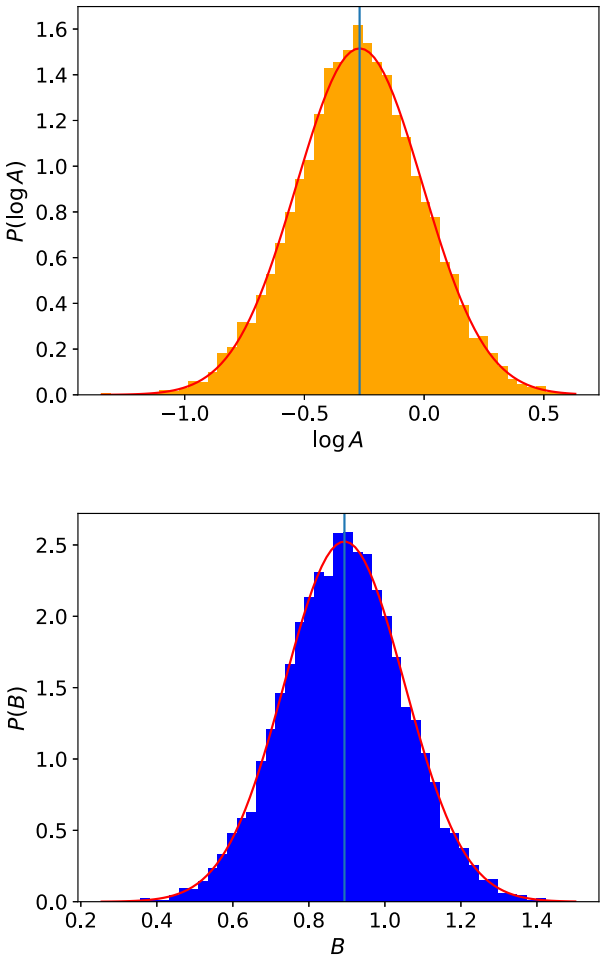

Figure 7. Probability distributions for the two parameters log A and B of the WHIM–LD scaling relation (equation 5), using smoothing $a = 1.2$.

Table 4. Best-fitting parameter values for selected smoothing scales.

Smoothing (Mpc)	log A	$\sigma_{\log A}$	B	σ_B
0.5	0.42	0.25	0.43	0.16
1.0	−0.19	0.26	0.82	0.16
1.2	−0.27	0.27	0.89	0.16
1.5	−0.32	0. 27	0.94	0.16
2.0	−0.30	0.28	0.97	0.17

the scaling relation is well within the statistical uncertainties of the scaling relation, the bias is systematic, in that the scaling relation always produces a lower estimated mass than the true one. As a result, such ∼10 per cent systematic bias must be corrected by boosting the inferred WHIM mass by +10 per cent. [1] Likewise, the effect of limiting the LD range to $\delta_{LD} = 1$–300 provides another systematic bias of approximately −5 per cent (2.15×10^{15} $M_\odot$ versus 2.08×10^{15} $M_\odot$), also qualitatively consistent with Fig. 4. This is also a systematic bias that needs to be corrected with an additional +5 per cent boost of the estimated mass. The combined effect of these two systematic biases is that the estimated masses must be corrected by +15 per cent, as also illustrated in Table 6.

[1]For larger values of the smoothing parameter, e.g. $a = 2$ Mpc, the reconstruction has a larger bias of up to −25 per cent, which is attributable to a larger fraction of the LD being moved outside of the WHIM filament regions by the wider smoothing kernel. Our analysis, however, does not support the use of such large smoothing kernels, and this larger bias is only reported as a caution against using too wide smoothing kernels.

3.4.2 *Choice of Bisous method of filament detection*

An additional source of systematic bias and error is the method of detection of WHIM filaments. As shown in Tuominen et al. (2021), the Bisous method successfully finds the vast majority (∼87 per cent) of the missing WHIM baryons outside the virial radii of galaxies and in the log $T(K) \geq 5.5$ range. This large 'capture' rate, using the Tuominen et al. (2021) terminology, indicates that the Bisous method leaves out a fraction of WHIM gas in the outskirts of the thickest filaments that are less correlated to the galaxy luminosity, and therefore not included in the estimate of the WHIM mass from the scaling relation. Although there is visual evidence that several filaments are somewhat wider than the Bisous–identified volumes, especially in the densest regions where the Bisous method does not have the flexibility to adapt its size (see discussion in Tuominen et al. 2021), we do not assess a correction to our estimates for this effect.

Moreover, Tuominen et al. (2021) compared the total hot WHIM mass in the EAGLE simulation within filaments detected with the Bisous and the NEXUX+ method, which is a different method of filament identification, and estimated a ±10 per cent difference between the two methods. It is therefore reasonable to assess a systematic error of ±10 per cent, in order to correct for the effects of the use of the Bisous method. A summary of the major sources of systematic error in the estimate of the WHIM masses from the LD-WHIM scaling relation is provided in Table 6.

3.4.3 *Other sources of systematic errors*

There are several other possible sources of systematic errors in the estimation of WHIM masses from the LD-WHIM density scaling relation. The comparison between the scaling relation derived from the earlier simulations used in Nevalainen et al. (2015) and the present EAGLE simulation is provided in Fig. 8. Despite the numerous differences between the two numerical simulations, which range from feedback methods to resolution etc., the two scaling relations are in statistical agreement.

When the EAGLE WHIM mass is reconstructed using the Nevalainen et al. (2015) scaling relation, instead of the EAGLE-derived relation, the mass is $2.5 \pm 0.5 \times 10^{15} M_\odot$, which is approximately 30 per cent larger that the one estimated in Table 5 according to the present scaling relation, although in statistical agreement within the uncertainties of the EAGLE simulations. This difference in reconstructed masses provides an estimate of the effect of other sources of systematic errors associated with the derivation of the WHIM–LD scaling relation. We therefore add a ±30 per cent systematic error to mass estimates from the LD-WHIM density scaling relation method as a means to address uncertainties associated with other prescriptions of the numerical simulations.

4 APPLICATION OF THE SCALING RELATION TO SDSS GALAXY FILAMENTS

In order to examine the performance of our simulation-based LD-WHIM density relation with real-life data, we applied it to the SDSS DR12 galaxy data (York et al. 2000; Ahn et al. 2014) that was previously analysed by Tempel et al. (2014b, 2016) and Kuutma

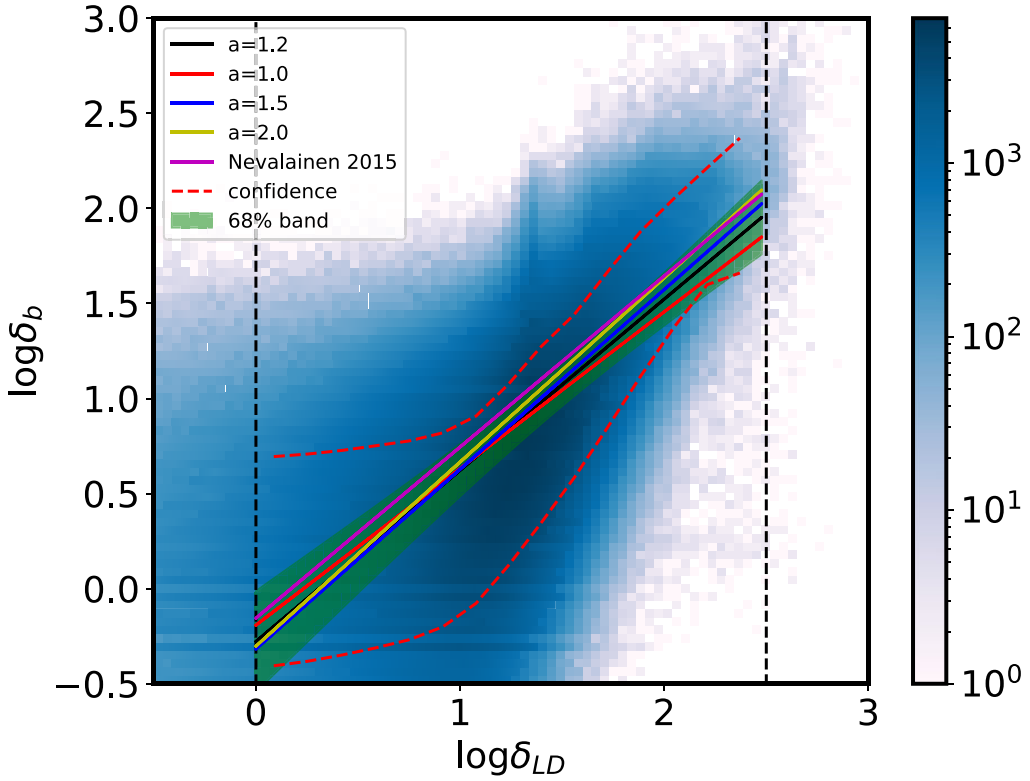

Figure 8. Best-fitting scaling relation between the galaxy luminosity density (LD) and the WHIM density for the nominal smoothing of $a = 1.2$ Mpc (black line), and for other values of the smoothing kernel, 1.0, 1.5, and 2.0 Mpc, indicated as solid black, red, and orange lines. The scaling relation obtained by Nevalainen et al. (2015), obtained from a different set of simulations, is also plotted for comparison in purple. The green band indicates the 68 per cent scatter interval of the power-law approximation to the LD–WHIM density relation. The red dashed lines indicate the 68 per cent scatter interval of the original data.

et al. (2020) to identify filament spines with the *Bisous* method (see Table 7 for the key features of the SDSS data used in this paper). The data correspond to the Legacy Survey, for a 7221 contiguous square degrees or 17.5 per cent of the full sky (Martínez et al. 2009). For this study, we consider only galaxies at redshifts $z = 0.02$–0.05, corresponding to a distance of approximately 88–220 Mpc for $H_0 = 67.8$ km s^{-1} Mpc^{-1}, as a volume-limited representative sample of the local Universe. A description of the selection of this volume-limited sample can be found in Tempel et al. (2014c). In brief, the choice of a low–redshift limit avoids the use of a local void that is underpopulated, and the upper limit mitigates the loss of low-luminosity galaxies, and the associated filaments, at higher redshift. This sample of galaxies is therefore intended to be representative of the low-redshift Universe, and its volume-limited nature makes the ensuing cosmological inferences straightforward. While the EAGLE and SDSS volumes differ by a factor of 8, the filament volume filling fractions are very similar, ∼5 per cent. Moreover, Fig. 11 shows that EAGLE and SDSS contain a comparable number of LD cells, after accounting for the volume difference.

We smoothed the measured *r*-band galaxy luminosity with our adopted $a = 1.2$ Mpc kernel (see Fig. 12 for a slice of the LD field). For a given pair of A and B values of the scaling relation (equation 6) of the Monte Carlo samples (see Section X), we then turned each LD value into WHIM density, and computed the total predicted WHIM mass in the SDSS filaments using

$$\log M_{\rm fil,SR} = \sum_{i=1}^{N_{\rm SDSS}} (\log A + B \log \delta_{\rm LD,i}) + \log \overline{\rho_b} + \log \Delta V_{\rm SDSS}, \quad (6)$$

where $\delta_{{\rm LD},\,i}$ is the measured luminosity overdensity in each of the $N_{\rm SDSS}$ cell of fixed volume $\Delta V_{\rm SDSS} = 0.2^3$ Mpc^3 within Bisous filaments. We repeated this for the 10 000 Monte Carlo samples obtaining a distribution of the predicted total WHIM mass in Bisous filaments in the SDSS volume (see Fig. 9). This yields WHIM mass of $\log M_{\rm fil,\,SR} = 16.02 \pm 0.11$, where the best-fitting value and there error are, respectively, the mean and standard deviation of the distribution. This value corresponds to approximately

$$M_{\rm fil,SR} = 1.054 \pm 0.265 \times 10^{16}\ {\rm M}_\odot.$$

This mass represents the WHIM in filaments as estimated from the LD-WHIM density scaling relation. However, prior to its use for cosmological inferences, it is necessary to remove the biases discussed in Section 3.4. Since the two sources of systematic bias, i.e. restriction to the $\delta_{\rm LD} = 1$–300 range and the LD smoothing which removes a fraction of the luminosity from the filament volume (see Table 6), require a combined correction by +15 per cent, the debiased WHIM mass inferred by our analysis becomes

$$M_{\rm fil,SR,corr} = 1.21 \pm 0.30 \times 10^{16}\ {\rm M}_\odot$$

The contribution of our predicted baryon content in the SDSS volume $V_{\rm SDSS}$ to the cosmic baryon budget is obtained as

$$\Omega_{\rm b,LD} = \frac{1}{\overline{\rho_b}} \frac{M_{\rm fil,SR,corr}}{V_{\rm SDSS}}. \quad (7)$$

The fraction of sky area covered by the SDSS's main footprint is 7221/41252.96 = 0.175, and therefore the volume between the two comoving radial distances $d_1 = 88$ Mpc and $d_2 = 220$ Mpc is given

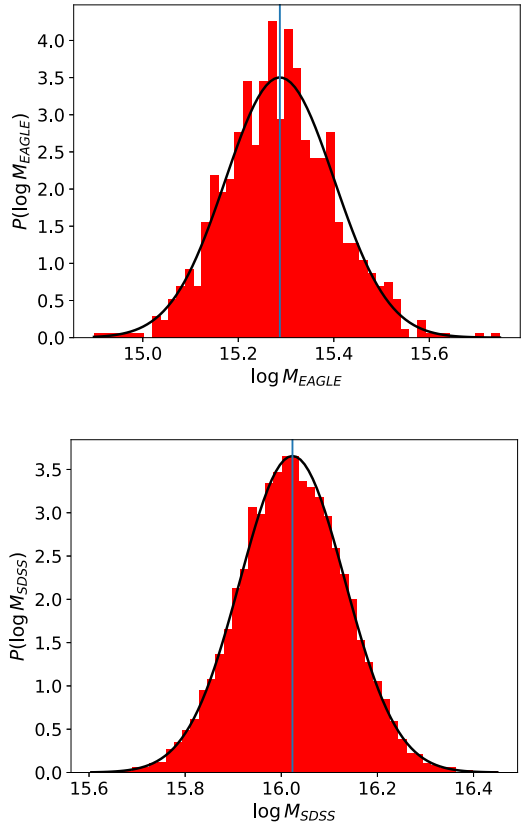

Figure 9. (a) Distribution of the predicted EAGLE WHIM mass in logarithmic scale, in units of $M_\odot$. The mean is 15.28, which converts to $1.9 \times 10^{15} M_\odot$. The mass distribution was obtained using all parameter values obtained from the Monte Carlo simulation. Overplotted is the best-fitting normal model. (b) Distribution of the predicted SDSS WHIM mass, with a mean of log M = 16.02. The mass distribution was obtained the same way as the EAGLE mass, using all parameter values obtained from the Monte Carlo simulation. Overplotted is the best-fitting normal model.

Table 5. Estimated WHIM mass in the EAGLE simulation using the various scaling relations.

a (Mpc)	EAGLE WHIM masses ($M_\odot$)		Prediction from SR
	No LD mask	LD mask	
0.5	2.15×10^{15}	1.31×10^{15}	$1.03 \pm 0.19 \times 10^{15}$
1.0	2.15×10^{15}	2.02×10^{15}	$1.85 \pm 0.39 \times 10^{15}$
1.2	2.15×10^{15}	2.08×10^{15}	$1.89 \pm 0.41 \times 10^{15}$
1.5	2.15×10^{15}	2.12×10^{15}	$1.8 \pm 0.41 \times 10^{15}$
2.0	2.15×10^{15}	2.14×10^{15}	$1.6 \pm 0.39 \times 10^{15}$

by

$$V_{\rm SDSS} = 0.175 \times \frac{4}{3}\pi \left(d_2^3 - d_1^3\right) = 6.84 \times 10^6 \ {\rm Mpc}^3.$$

In terms of Ω_b, our prediction for the SDSS WHIM density translates to

$$\Omega_{\rm b,LD} = (0.31 \pm 0.07 \pm 0.12)\ \Omega_b, \quad (8)$$

where the best-fitting value is bias-corrected, and the additional sources of systematic error described in Section 3.4 were added to the statistical errors associated with the determination of the scaling relation.

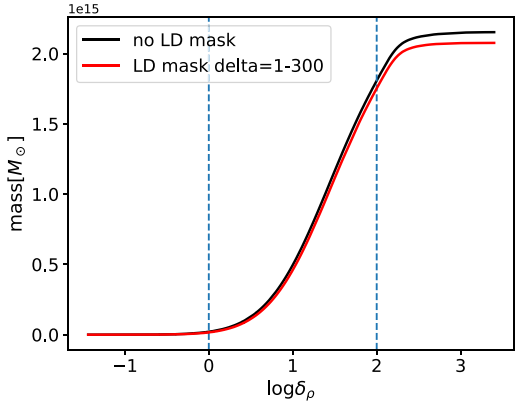

Figure 10. Cumulative distribution of the true EAGLE WHIM mass in filaments, for a smoothing parameter $a = 1.2$ Mpc.

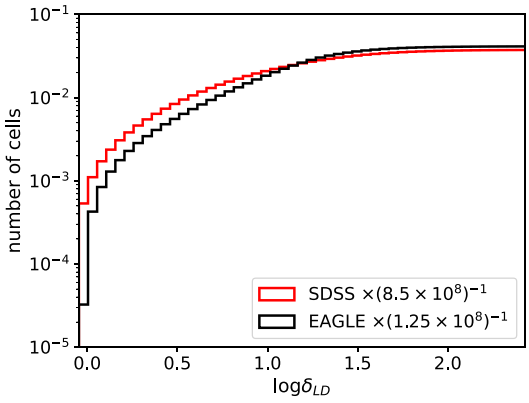

Figure 11. Cumulative distribution of the density of LD cell counts in filaments, for EAGLE and SDSS. The number of cells was rescaled by the volume of each data set, indicating that EAGLE contains approximately 15 per cent more LD cells, per unit volume, than SDSS.

This result indicates that if our EAGLE-based LD-WHIM density relation accurately describes the real universe, the baryon content of the SDSS volume traceable by our methods corresponds to a substantial fraction of the expected cosmic baryon density. Additionally, our result is consistent with the current estimates of the observationally missing baryons (Shull, Danforth & Tilton 2014; Danforth et al. 2016). This implies that our updated relation, together with the Bisous filament finder and the LD field method, may be a useful tool for the missing baryon searches.

5 DISCUSSION AND CONCLUSIONS

This paper has presented an update to the Nevalainen et al. (2015) method to trace cosmic baryons with the use of optical light from galaxy surveys, with the use of EAGLE numerical simulations. The technique studies the correlation between the optical luminosity density of galaxies and the WHIM density in galaxy filaments that are identified by the *Bisous* method, with the goal to predict WHIM masses in galaxy filaments. The first result of our analysis is that the EAGLE simulations predict a strong correlation between the WHIM gas density and the smoothed galaxy luminosity density in filaments, confirming the earlier funding of Nevalainen et al. (2015) based on lower resolution simulations. This is consistent with the scenario whereby both the diffuse WHIM gas and the stellar component in the

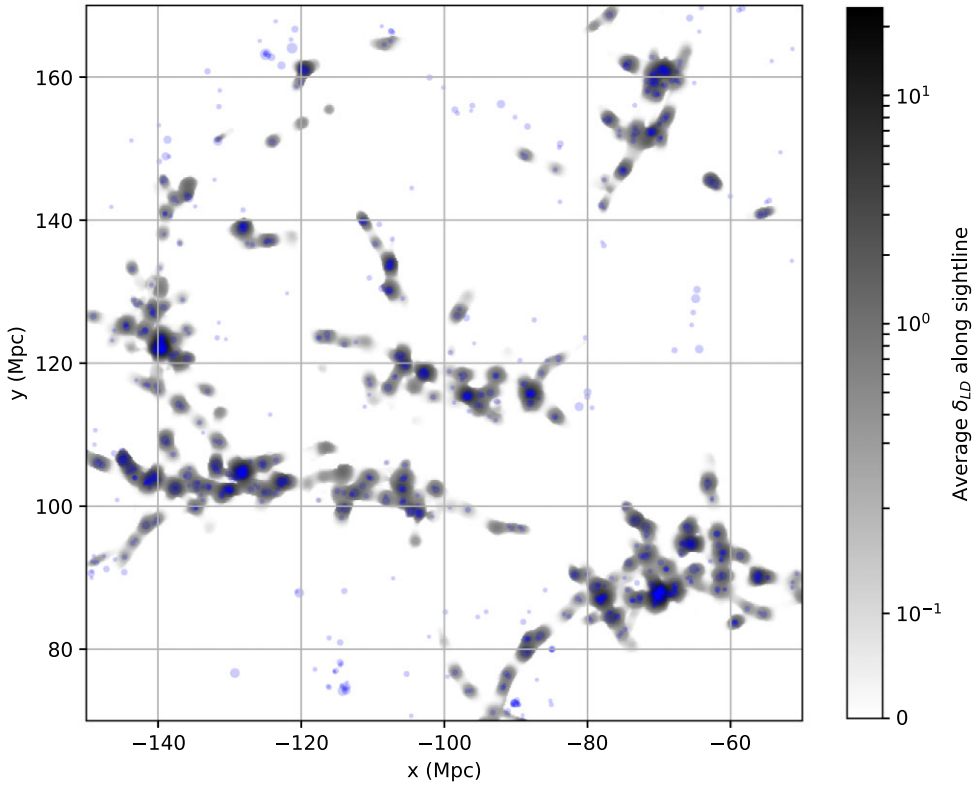

Figure 12. Image of a 100 × 100 Mpc^2 portion of the SDSS, with LD intensities averaged along a depth of 5 Mpc. The grey-scale cells represent the smoothed LD in the *Bisous* filaments, and the blue dots represent the SDSS galaxies (larger circles represent higher *r*-band luminosity) used to identify the filaments.

Table 6. Major sources of systematic bias and errors associated with the LD-WHIM scaling relation. All biases systematically underpredict the WHIM mass, and therefore a positive correction is required to offset this bias.

Source of systematic bias and error	Effect on WHIM mass
Systematic biases	
Choice of LD boundaries	−5 per cent
Use of $a = 1.2$ Mpc smoothing kernel	−10 per cent
Summary of correction for systematic biases	+15 per cent
Systematic uncertainties	
Choice of filament detection method	±10 per cent
Other choices in the numerical simulations	±30 per cent

Table 7. Key parameters of the SDSS DR12 legacy survey galaxies used in this paper and Tempel et al. (2014b).

Redshift boundaries	0.02–0.05 (88–220 Mpc)
Contiguous sky area covered	7221 deg^2
Number of galaxies with $M_r \leq -19.5$	55973
Average <LD>	$1.1 \times 10^8\ L_\odot$ Mpc^{-3}
Fraction of volume occupied by WHIM filaments in SDSS and EAGLE	5.0 per cent
Fraction of volume occupied by WHIM filaments in SDSS ($\delta_{\rm LD} = 1$–300)	3.7 per cent
Fraction of volume occupied by WHIM filaments in EAGLE ($\delta_{\rm LD} = 1$–300)	4.2 per cent

galaxies trace the same underlying dark matter density field, enabling the usage of the relatively easily observable galaxy luminosities in spectroscopic surveys as a tracer of the more hard-to-detect WHIM.

We then established a new LD-WHIM density scaling relation based on the EAGLE simulations. The 68 per cent scatter in the scaling relation at a fixed value of the luminosity density is less than $\frac{1}{2}$ dex, throughout the range of the luminosity densities under consideration (i.e. overdensities of $\delta_{\rm LD} = 1$–300). This is a manageable amount of scatter, and it endows the scaling relation with the power to make meaningful predictions for the WHIM mass, based on the unrelated luminosity density observable.

We applied the scaling relation to a sample of low-redshift galaxies ($0.02 \leq z \leq 0.05$) from the SDSS DR12 Legacy data, for which Tempel et al. (2014b) had already identified Bisous filaments, in an area that covers ~ 17.5 per cent of the sky. Our analysis predicts that the optical luminosity of filaments, outside of the virial radii of the galaxies, traces approximately $\Omega_{\rm b,\,LD} \simeq 31 \pm 10$ per cent of the cosmological density of baryons Ω_b. This is consistent with the current estimates of the observationally missing baryons. Thus, assuming that our EAGLE-based relation accurately captures the real universe, our method has the potential to address the missing baryon search.

The main motivation for this LD-WHIM scaling relation is to make predictions of the WHIM density for filaments detected in large portions of the sky by, e.g. the SDSS and by upcoming 4MOST surveys (Winkler et al. 2020), in order to identify the most promising sight-lines for follow–up observations in the FUV and X-rays (e.g. with Athena, Barret et al. 2020). In this case, the LD-WHIM scaling relation may become the tool of choice to implement a synergy between the relatively inexpensive optical observations of galaxies and the more challenging FUV and X-ray follow-ups, which can be

used to confirm the nature of the WHIM only for the sight-lines with the largest predicted column density of WHIM.

DATA AVAILABILITY

The EAGLE data underlying this article are available from the Virgo Consortium at http://virgodb.dur.ac.uk/ (McAlpine et al. 2016; The EAGLE team 2017), and from the SDSS project at https://www.sdss.org/ (for DR12, see Alam et al. 2015). Processed data and tables presented in the paper are accessible upon request to the authors.

REFERENCES

Ahn C. P. et al., 2014, ApJS, 211, 17
Ahoranta J. et al., 2020, A&A, 634, A106
Alam S. et al., 2015, ApJS, 219, 12
Barret D., Decourchelle A., Fabian A., Guainazzi M., Nandra K., Smith R., den Herder J.-W., 2020, Astron. Nachr., 341, 224
Bertone S., Schaye J., Dolag K., 2008, Space Sci. Rev., 134, 295
Bonamente M., 2017, Statistics and Analysis of Scientific Data: Graduate Texts in Physics, Second Edition. Springer, Berlin
Bonamente M., Nevalainen J., Tilton E., Liivamägi J., Tempel E., Heinämäki P., Fang T., 2016, MNRAS, 457, 4236
Camps P. et al., 2018, ApJS, 234, 20
Cen R., Ostriker J. P., 1999, ApJ, 514, 1
Crain R. A. et al., 2015, MNRAS, 450, 1937
Cui W., Borgani S., Dolag K., Murante G., Tornatore L., 2012, MNRAS, 423, 2279
Danforth C. W. et al., 2016, ApJ, 817, 111
Davé R. et al., 2001, ApJ, 552, 473
Fang T., Buote D. A., Humphrey P. J., Canizares C. R., Zappacosta L., Maiolino R., Tagliaferri G., Gastaldello F., 2010, ApJ, 714, 1715
Galárraga-Espinosa D., Aghanim N., Langer M., Gouin C., Malavasi N., 2020, A&A, 641, A173
Galárraga-Espinosa D., Aghanim N., Langer M., Tanimura H., 2021, A&A, 649, A117
Kuutma T., Poudel A., Einasto M., Heinämäki P., Lietzen H., Tamm A., Tempel E., 2020, A&A, 639, A71
Liivamägi L. J., Tempel E., Saar E., 2012, A&A, 539, A80
Martínez V. J., Arnalte-Mur P., Saar E., de la Cruz P., Pons-Bordería M. J., Paredes S., Fernández-Soto A., Tempel E., 2009, ApJ, 696, L93
Martizzi D. et al., 2019, MNRAS, 486, 3766
McAlpine S. et al., 2016, Astron. Comput., 15, 72
Muru M., Tempel E., 2021, A&A, 649, A108
Nevalainen J. et al., 2015, A&A, 583, A142
Nicastro F. et al., 2018, Nature, 558, 406
Penton S. V., Shull J. M., Stocke J. T., 2000, ApJ, 544, 150
Pillepich A. et al., 2018, MNRAS, 473, 4077
Planck Collaboration XVI, 2014, A&A, 571, 16
Schaye J. et al., 2015, MNRAS, 446, 521
Shull J. M., Smith B. D., Danforth C. W., 2012, ApJ, 759, 23
Shull J. M., Danforth C. W., Tilton E. M., 2014, ApJ, 796, 49
Springel V., 2005, MNRAS, 364, 1105
Stocke J. T., Penton S. V., Danforth C. W., Shull J. M., Tumlinson J., McLin K. M., 2006, ApJ, 641, 217
Stoica R. S., Martínez V. J., Saar E., 2007, J. R. Stat. Soc. C, 56, 1
Tchernyshyov K. et al., 2022, ApJ, 927, 147T
Tempel E. et al., 2014c, A&A, 566, A1
Tempel E., Stoica R. S., Martínez V. J., Liivamägi L. J., Castellan G., Saar E., 2014a, MNRAS, 437, L11
Tempel E., Stoica R. S., Martínez V. J., Liivamägi L. J., Castellan G., Saar E., 2014b, MNRAS, 438, 3465
Tempel E., Kipper R., Tamm A., Gramann M., Einasto M., Sepp T., Tuvikene T., 2016, A&A, 588, A14
The EAGLE team, 2017, preprint (arXiv:1706.09899)
Tuominen T. et al., 2021, A&A, 646, A156
Winkler R., Micheva G., Frey S., Bellido-Tirado O., deJong R., 2020, in Proc. SPIE Conf. Ser. Vol. 11450, Modeling, Systems Engineering, and Project Management for Astronomy IX. SPIE, Bellingham, p. 114502K
York D. G. et al., 2000, AJ, 120, 1579

This paper has been typeset from a TEX/LATEX file prepared by the author.